# Measurements of $g$ factors and lifetimes of low lying states in $^{58-64}$Ni and their shell model implications

O. Kenn,[1] K.-H. Speidel,[1] R. Ernst,[1] J. Gerber,[2] P. Maier-Komor,[3] and F. Nowacki[4]
[1]*Institut für Strahlen- und Kernphysik, Universität Bonn, Nußallee 14-16, D-53115 Bonn, Germany*
[2]*Institut de Recherches Subatomique, F-67037 Strasbourg, France*
[3]*Physik-Department, Technische Universität München, James-Franck-Str., D-85748 Garching, Germany*
[4]*Laboratoire de Physique Théorique, 3-5 rue de l'Université, F-67084 Strasbourg Cedex, France*
(Received 5 December 2000; revised manuscript received 18 January 2001; published 2 May 2001)

$g$ factors have been measured for the first $2^+$ states of $^{58,60,62,64}$Ni isotopes employing the combined technique of projectile Coulomb excitation and transient magnetic fields. Lifetimes of low-lying states were redetermined using the Doppler shift attenuation method technique. The same target has been used in all measurements and the isotopes were provided by the ion source of the accelerator. These conditions guarantee high reliability and precision as demonstrated in earlier experiments. The measured $g$ factors and the deduced $B(E2)$ values are well explained by large scale shell model calculations in which valence particles are strongly coupled to an excited $^{56}$Ni core.

DOI: 10.1103/PhysRevC.63.064306 PACS number(s): 21.10.Ky, 25.70.De, 27.50.+e

## I. INTRODUCTION

Magnetic moments of nuclear states are particularly sensitive to the detailed composition of the wave function and the particle (proton/neutron) nature as well, because of the specific difference in sign and magnitude of the spin $g$ factors of the two nucleons [$g_s(p)=+5.586$, $g_s(n)=-3.826$]. This unique feature has been extensively used for the study of the light $fp$ shell nuclei Ti and Cr for which highly meaningful shell model calculations in a rather large configuration space are available [1–3]. Comparison between precise experimental data and theoretical values allows for a stringent test not only of the model space but also of the effective $NN$ interactions used in the calculations. It was found that the large scale shell model explains rather well both the $g$ factors and the $B(E2)$ values for the low-lying states of $^{50}$Cr and $^{52}$Cr. In particular, the larger $g$ factor of the $4_1^+$ state relative to the $2_1^+$ state in $^{50}$Cr is in excellent agreement with the shell model prediction which includes the excitation of $f_{7/2}$ particles to the remaining $fp$ shell orbits. In contrast, the high precision $g$ factors for the Ti isotopes $^{46,48,50}$Ti exhibit distinct deviations from the model expectations. These deviations are attributed to excitations of the $^{40}$Ca core and/or deficits in the effective interactions [3].

For heavier $fp$ shell nuclei in the iron, cobalt and nickel region, shell model calculations have been performed by several groups [4–6] in the past to describe many experimental data. It was emphasized already in these earlier calculations that the excitation of both protons and neutrons from the $0f_{7/2}$ shell to the higher orbitals of the $fp$ shell is an essential feature of the nuclear structure.

With respect to the experimental data, in particular for the Ni isotopes, $g$ factors were determined for the first $2^+$ states with relatively low precision [7]. However, the $g$ factors of the $(3/2)^-$ ground states and first excited $(5/2)^-$ states of the odd Ni isotopes have been measured with high precision [8]. The shell model interpretation of the odd nuclei is based on distinct single neutron configurations, $1p_{3/2}$ and $0f_{5/2}$, in the wave function as the $g$ factors are definitely negative for the $(3/2)^-$ states and positive for the $(5/2)^-$ states. The situation is not so clear for the even isotopes where the $g$ factor of the $2_1^+$ state rises from a possibly negative value for $^{58}$Ni to large, positive, values for the heavier isotopes suggesting an increase of collectivity toward $g=Z/A=0.44$ departing from the $N=28$ shell closure. Unfortunately, the existing data have large errors which do not allow us to draw definite conclusions. In any case, most of the theoretical calculations predict a negative $g$ factor for the $2_1^+$ state of $^{58}$Ni, in accordance with the experimental value [6]. In view of the existing uncertainties, a redetermination of the $g$ factors of the first $2^+$ states of all even Ni isotopes under improved experimental conditions was highly desirable. To achieve this goal, the newly developed technique of projectile Coulomb excitation in inverse kinematics combined with transient magnetic fields has been used [9,10]. In addition, lifetimes of excited states were redetermined employing the Doppler shift attenuation method (DSAM). Like in former experiments on Ti, Cr [1,2], and Se [9], the nuclei of interest were provided as isotopically pure beams by the ion source of the accelerator.

The essence of these investigations has already been reported as a rapid communication [11]. The present paper is dedicated to more details of the spectroscopy.

## II. EXPERIMENTAL DETAILS

In the present measurements, beams of $^{58}$Ni and $^{60}$Ni in their natural isotopic abundance and enriched $^{62}$Ni and $^{64}$Ni were provided by the ion source of the Munich tandem accelerator and accelerated to energies of 155 and 160 MeV, with intensities of about 1 pnA on the target. The target consisted of several layers: a 0.45 mg/cm$^2$-thick layer of natural carbon was deposited on a 3.82 mg/cm$^2$ gadolinium layer which had been evaporated on a 1 mg/cm$^2$ tantalum foil; the tantalum was backed by a 3.5 mg/cm$^2$ copper layer to provide good thermal conductivity to the whole target. For

 

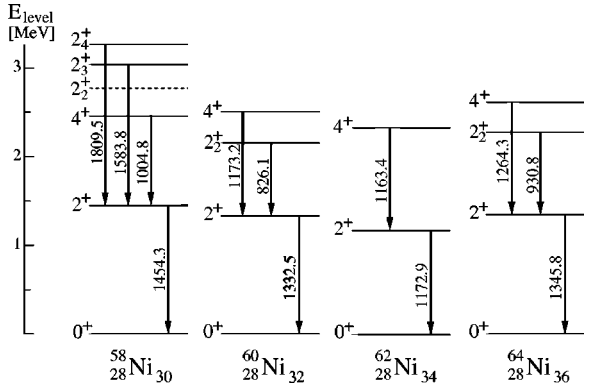


FIG. 1. Low-lying states of $^{58,60,62,64}$Ni [17–20]. The $2_2^+$ level of $^{58}$Ni has not been seen in the present measurements (see Fig. 3).

the gadolinium evaporation, the tantalum foil was kept at a temperature of 800 K to ensure good magnetic properties of the gadolinium [12]. The copper backing also served as a stopper for the Coulomb excited Ni ions in a hyperfine interaction-free environment. The nuclei excited in the carbon layer (Fig. 1) traversed the gadolinium layer with mean velocities of 0.036*c* in which they experienced the transient field, and were stopped in the copper backing after traversal through the thin tantalum layer. The target was cooled to liquid nitrogen temperature and magnetized by an external field of 0.06.

The $\gamma$ rays emitted from the excited states were measured in coincidence with the forward scattered carbon ions using $9\times9$-cm $BaF_2$ scintillators. In addition, an *n*-type, coaxial Ge detector with a relative efficiency of 23% was placed at 0° to the beam direction to serve as a monitor for contaminant lines and to measure nuclear lifetimes via the DSAM technique. The high energy $\gamma$ rays from $^{12}$C target excitation ($2_1^+\rightarrow0_1^+$:4.43 MeV) were weak and therefore contributed only a negligible background in the energy region of interest. Ions were registered in a 100-$\mu$m-thick Si detector placed at 0° and subtending an angle of $\pm20°$. For this purpose the beam had to be stopped in a tantalum foil whose thickness was such that the carbon ions could easily pass through to the Si detector. The latter was operated throughout the measurements at a low bias ($\simeq5$ V) to separate light charged particles such as protons and alphas (which do not stop completely) from the carbon ions. The light particles result from sub-Coulomb transfer and fusion reactions with the carbon target which may contribute background $\gamma$ rays to the coincidence spectra. Figure 2 shows a particle spectrum taken in coincidence with all $\gamma$ rays in the presence of a $^{58}$Ni beam. The low energy peak was attributed to $\alpha$ particles corresponding to $^{62}$Zn nuclei produced in an $\alpha$-transfer reaction from the examination of the observed $\gamma$-ray spectrum in coincidence with particles in the peak (see below). This procedure of discriminating against light particles has already been successfully used in earlier experiments [3]. It should be noted that the same structure of the particle spectrum was obtained with all Ni beams whereby the low energy peak was always associated with the corresponding Zn isotope: $^{62}$Zn was formed with $^{58}$Ni and $^{68}$Zn with $^{64}$Ni beams. By gating on the carbon peak of the particle spectrum, *only* $\gamma$

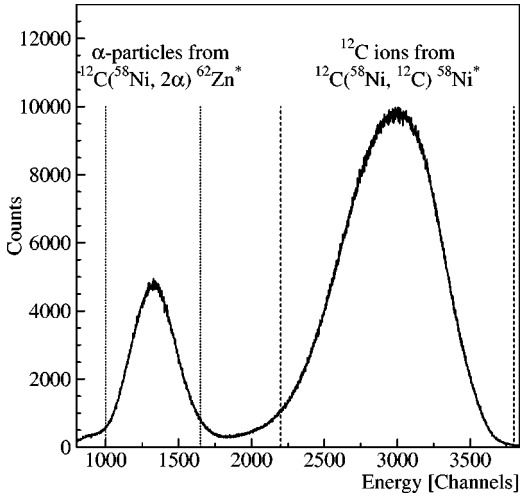


FIG. 2. Particle spectrum with a 100 $\mu$m Si detector at low bias. The $\alpha$ particles are well separated from the carbon ions.

rays from Coulomb excitation of the Ni projectiles appear in the coincidence spectrum. Hence the relatively poor energy resolution of the $BaF_2$ scintillators was not an impediment to obtaining a clean spectroscopy.

Figures 3 and 4 show typical $\gamma$-ray spectra of the Ge detector and the $BaF_2$ scintillator, respectively, in coincidence with carbon ions using a $^{58}$Ni beam.

A $\gamma$-coincidence spectrum obtained with $^{58}$Ni projectiles by gating with $\alpha$ particles shows characteristic $\gamma$-ray lines of $^{62}$Zn following an $\alpha$ transfer from carbon to $^{58}$Ni (Fig. 5). The remaining $2\alpha$ particles from the $^8$Be decay are registered in the Si detector leading to the $^{62}$Zn spectrum. Evidently, the strongest $\gamma$-ray line refers to the ($2_1^+\rightarrow0_1^+$) transition and higher excited states are only weakly populated. This feature provides a clear signature for the particle transfer character of the nuclear reaction which was studied in an earlier experiment [13] and is quite different from a fusion reaction. The simple structure of the $^{62}$Zn spectrum stimulated a first measurement of the *g* factor of the 0.954 MeV,

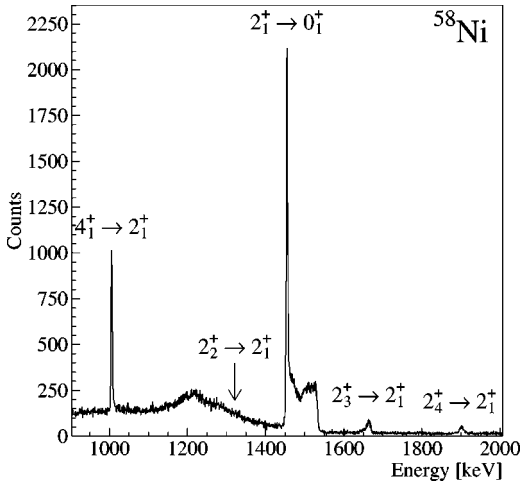


FIG. 3. $^{58}$Ni $\gamma$-ray spectrum observed with the Ge detector in coincidence with the high energy peak in the particle spectrum corresponding to C ions.

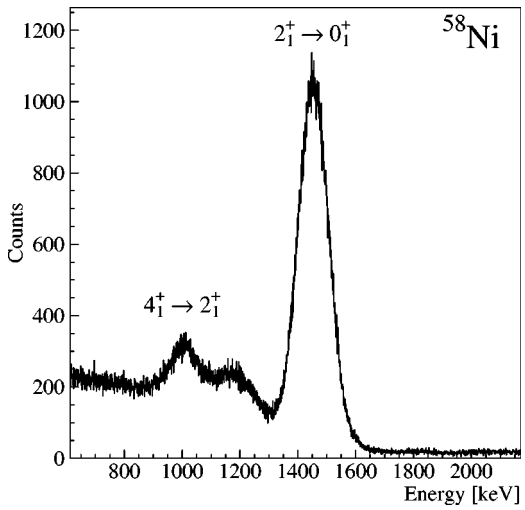


FIG. 4. $^{58}$Ni $\gamma$-ray spectrum observed with the $BaF_2$ detector in coincidence with the high energy peak in the particle spectrum corresponding to C ions.

$\tau = 4.3(3)$ ps, $2_1^+$ state since feeding from high-lying states is negligibly small. Details of this experiment will be reported in a forthcoming publication [14].

Particle-$\gamma$ angular correlations $W(\theta_\gamma)$ and anisotropies $W(\theta_\gamma = 50°)/W(\theta_\gamma = 80°)$ have been measured for the $(2_1^+ \rightarrow 0_1^+)$ transition of each nucleus in order to determine the logarithmic slopes, $S = [1/W(\theta_\gamma)] \cdot [dW(\theta_\gamma)/d\theta_\gamma]$ in the rest frame of the $\gamma$ emitting nuclei at the angle $\theta_\gamma = 65°$ where the experimental sensitivity to the precessions was optimal (Ref. [2] and Table I). Figure 6 shows a detailed angular correlation for the $^{58}$Ni$(2_1^+ \rightarrow 0_1^+)$ transition.

Precession angles $\Phi^{exp}$ were derived from double ratios $DR(i/j) = (N_i\uparrow/N_i\downarrow)/(N_j\uparrow/N_j\downarrow)$ of coincident counting rates $N$ with an external field applied perpendicular to the

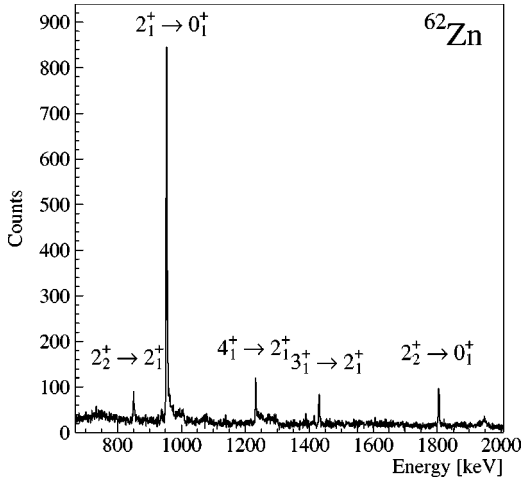


FIG. 5. $\gamma$ rays observed with the Ge detector in coincidence with particles associated with the low energy peak in the particle spectrum (Fig. 2). The $\gamma$ spectrum shows that the low energy peak indeed corresponds to $\alpha$ particles and all $\gamma$-ray lines identified belong to the deexcitation of $^{62}$Zn states populated in the $\alpha$-transfer reaction.

$\gamma$-detection plane, alternately in the ''up''and ''down'' directions. The indices $i,j$ represent a pair of $\gamma$ detectors symmetric to the beam axis. The precession angles are given by [2]

$$\Phi^{exp} = \frac{1}{S} \cdot \frac{\sqrt{DR}-1}{\sqrt{DR}+1} = g \cdot \frac{\mu_N}{\hbar} \int_{t_{in}}^{t_{out}} B_{TF}[v_{ion}(t)] \cdot e^{-t/\tau} dt, \tag{2.1}$$

where $g$ is the $g$ factor of the $2_1^+$ state and $B_{TF}$ is the transient field acting for the time $(t_{out}-t_{in})$ while the ions traverse the gadolinium layer; the exponential accounts for the decay of the $2_1^+$ state with lifetime $\tau$.

The lifetimes of most excited states have been measured simultaneously using the DSAM technique with the 0° Ge detector. The high ion velocities (see Table I) implied high sensitivity for the lifetimes in the picosecond range. The Doppler-broadened shapes of the emitted $\gamma$-ray lines were fitted for the known reaction kinematics applying stopping powers [15] to Monte Carlo simulations including the second order Doppler effect as well as the finite size and energy resolution of the Ge detector. The feeding from higher states was also taken into account. The computer code LINESHAPE [16] was used in the analysis. The high quality of the lineshape fits obtained is shown in Fig. 7. Characteristic structures in the line shape due to differences in the slowing down of the ions in the different target layers were well reproduced. The measured lifetimes are summarized in Table II together with values quoted in the literature.

## III. RESULTS

The $g$ factors were derived from the experimental precession angles $\Phi^{exp}$ by determining the effective transient field $B_{TF}$ on the basis of the empirical linear parametrization [2]:

$$B_{TF}(v_{ion}) = G_{beam} \cdot B_{lin} \tag{3.1}$$

with

$$B_{lin} = a(Gd) \cdot Z_{ion} \cdot \frac{v_{ion}}{v_0}, \tag{3.2}$$

where the strength parameter $a(Gd) = 17(1)$ T [2], $v_0 = e^2/\hbar$, and $G_{beam} = 0.69(6)$ is the attenuation factor accounting for the dynamic demagnetization of the gadolinium induced by the ion beam [21]. The $G_{beam}$ value was determined on the basis of many experimental data which describe the dependence of the attenuation on parameters such as the stopping power and intensity of the beam ions in the gadolinium host, as well as on the electron orbitals of the projectile ions which are responsible for the transient field strength as well [3,22]. In fact, the mean stopping power of the Ni ions in gadolinium was, at their respective energies, $\langle dE/dx \rangle \simeq 12$ MeV/$\mu$m. Moreover, the mean velocities of the excited ions in the ferromagnet (Table I) relative to the Bohr velocities of the electrons in the $2s$ and $3s$ orbitals, $\langle v_{ion}/v_{2sBohr} \rangle = 0.6$ and $\langle v_{ion}/v_{3sBohr} \rangle = 1.7$, show that both electron configurations determine the ion fractions for the

TABLE I. Summary of the average velocities of the ions entering, exiting, and traversing the ferromagnetic foil, the measured logarithmic slopes of the angular correlations at $|\theta_\gamma| = 65°$, and the precession angles $\Phi^{exp}$. The $\Phi^{lin}/g$ values were calculated using Eqs. (2.1), (3.1), and (3.2). The measurement on $^{56}$Fe($2_1^+$) served as a calibration of the transient field (see text).

| Nucleus | $E_x(2_1^+)$ [MeV] | $\langle v/v_0\rangle_{in}$ | $\langle v/v_0\rangle_{out}$ | $\langle v_{ion}/v_0\rangle$ | $\lvert S(65°)\rvert$ | $\Phi^{exp}$ [mrad] | $\frac{\Phi^{lin}}{g}$ [mrad] |
|---|---|---|---|---|---|---|---|
| | | 6.5 | 3.3 | 4.9 | 2.336(31) [a] | 1.74(68) | 28.2(2.5) |
| $^{58}$Ni | 1.454 | 6.6 | 3.5 | 5.0 | 2.415(17) [b] | 0.92(30) | 28.4(2.5) |
| | | 6.4 | 3.2 | 4.8 | 2.482(21) [a,c] | 1.12(38) | 28.2(2.5) |
| $^{60}$Ni | 1.333 | 6.5 | 3.4 | 4.9 | 2.381(45) | 4.59(71) | 28.9(2.5) |
| $^{62}$Ni | 1.173 | 6.5 | 3.5 | 4.9 | 2.329(47) | 5.10(60) | 30.6(2.7) |
| $^{64}$Ni | 1.346 | 6.4 | 3.6 | 4.9 | 2.413(46) | 5.51(80) | 29.8(2.6) |
| $^{56}$Fe | 0.847 | 6.6 | 3.5 | 4.9 | 1.871(25) | 19.4(1.3) | 31.6(4.6) |

[a]Beam energy 155 MeV.
[b]Beam energy 160 MeV.
[c]Vertical mask in front of the particle detector.

transient field strength as well as for the beam induced attenuation. In addition, the magnitude of $G_{beam}$ was reconfirmed through a precession measurement on the first $2^+$ state of $^{56}$Fe whose $g$ factor is $g = 0.61(8)$ [8] (Table I). In this experiment, the same target was bombarded with $^{56}$Fe beams of 155 MeV which refers to ion conditions very similar to those pertaining to the Ni beams. An attenuation factor of $G_{beam} = 0.69(10)$ was obtained which is in excellent agreement with the adopted value.

The precession data are summarized in Table I. Beam bending effects were negligible due to effective shielding of the stray magnetic field. The precision of the $^{58}$Ni($2_1^+$) precession was improved by two additional measurements. In one of these, the beam energy was increased to 160 MeV yielding a higher excitation cross section. Furthermore, the $\gamma$-ray anisotropy was enhanced by inserting a vertical mask in front of the Si detector [23]. The precessions $\Phi^{lin}/g$ listed in the table were calculated using Eqs. (2.1), (3.1), and (3.2). Table II summarizes the $g$ factors and the $B(E2)$'s from the measured lifetimes.

Significant differences are found in the lifetimes between the present measurements and values quoted in the literature in particular for the $2_1^+$ and $4_1^+$ states of $^{60}$Ni. In general, all $2_1^+$ lifetimes are slightly longer than the literature values with the exception of $^{62}$Ni($2_1^+$) where the lifetime was confirmed. For the $4_1^+$ states of $^{58}$Ni and $^{64}$Ni, where only lower limits of lifetimes were known, definite values have now been obtained. It should be noted that the sensitivity and

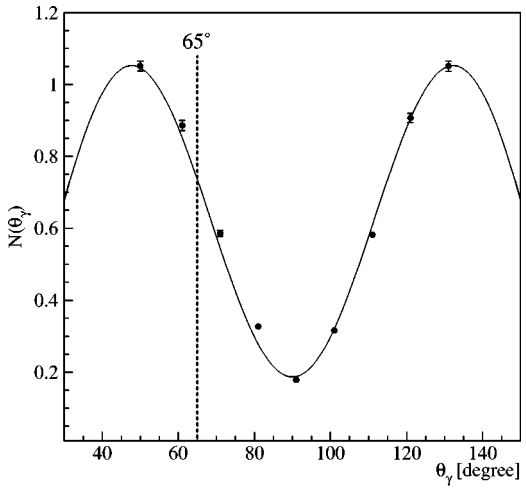


FIG. 6. Measured $\gamma$-angular correlation for the $^{58}$Ni($2_1^+ \rightarrow 0_1^+$) transition with a least squares fit to the data. The dashed line at $\theta_\gamma = 65°$ refers to the detector position for the precession measurements (see text).

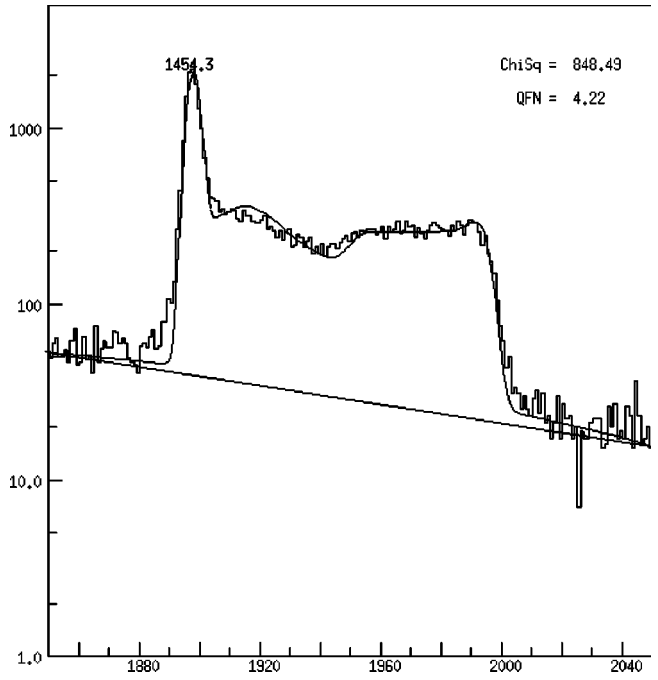


FIG. 7. DSAM fit to the Doppler broadened shape of the ($2_1^+ \rightarrow 0_1^+$) $\gamma$ line of $^{58}$Ni including a linear background.

TABLE II. Comparison of the measured $g$ factors, lifetimes, and $B(E2)$'s to earlier data and to results from large-scale shell model (SM) calculations in which $t=5$ nucleons were excited from the $0f_{7/2}$ shell to the remaining $fp$ shell orbits.

| Nucl.$(I^\pi)$ | $\tau$ [ps] | | $B(E2)$ [W.u.] | | $g(2_1^+)$ | | |
|---|---|---|---|---|---|---|---|
| | Refs. [17–20] | present | present | $SM_{t=5}$ | Ref. [7] | present | $SM_{t=5}$ |
| $^{58}$Ni$(2_1^+)$ | 0.96(4) | 1.27(2) | 7.4(1) | 6.60 | −0.06(12) | 0.0378(85) | 0.0350 |
| $(4_1^+)$ | $\geqslant$1.4 | 5.4(6) | 11(1) | | | | |
| $(2_3^+)$ | 0.075(14) | 0.108(10) | 1.4(4) [a] | | | | |
| $(2_4^+)$ | 0.050(4) | 0.076(12) | 5(4) [b] | | | | |
| $^{60}$Ni$(2_1^+)$ | 1.03(2) | 1.31(3) | 10.6(2) | 9.39 | 0.09(12) | 0.158(28) | 0.0975 |
| $(4_1^+)$ | 1.6(4) | 4.8(1.5) | 6(2) | | | | |
| $^{62}$Ni$(2_1^+)$ | 2.09(3) | 2.01(7) | 12.5(4) | 10.02 | 0.33(12) | 0.167(24) | 0.2050 |
| $^{64}$Ni$(2_1^+)$ | 1.27(4) | 1.57(5) | 7.7(3) | 5.33 | 0.45(12) | 0.184(31) | 0.1405 |
| $(4_1^+)$ | $\geqslant$0.45 | 2.5(4) | 6.6(1.0) | | | | |

[a] $\delta(2_3^+ \rightarrow 2_1^+) = +0.21(3)$ (Ref. [17]).
[b] $\delta(2_4^+ \rightarrow 2_1^+) = +0.7(4)$ (Ref. [17]).

reliability of the present experiments were substantially increased due to the high ion velocities.

## IV. DISCUSSION

The experimental $2_1^+$ $g$ factors and $B(E2)$ values of the $(2_1^+ \rightarrow 0_1^+)$ transitions were compared with results from large scale shell model calculations in the $fp$ shell configuration space. These calculations were performed with the computer code ANTOINE [24] using a modified version of the Kuo-Brown effective interaction KB3 [25]. The same procedure was applied earlier to describe similar data for Ti and Cr isotopes [1,2].

Both $g$ factors and $B(E2)$'s are well reproduced by the calculations. As shown in Figs. 8 and 9 good agreement with the experimental values is only achieved with excitations of $t$ nucleons from the $0f_{7/2}$ orbit to the $1p_{3/2}$, $0f_{5/2}$, and $1p_{1/2}$ orbits. The most striking result emerges for $^{58}$Ni$(2_1^+)$, with its small but definitely positive $g$ factor: $g(2_1^+) = +0.0378(85)$. In this particular case, the calculated $g$ factors evolve from negative values for $t=0$ and $t=2$ excitations to positive values which finally converge for $t=5$ to the experimental value. For all other isotopes the agreement between theory and the experimental data is nearly of the same quality, but, as the $g$ factors are all positive, the dependence on the number of excited particles is less dramatic than for $^{58}$Ni. A full calculation was carried out for $^{64}$Ni$(2_1^+)$ which very well agrees with the $t=5$ result. It is also evident that for an inert $f_{7/2}$ shell ($t=0$), the calculations generally overestimate the $g$ factors supporting the presence of a strong coupling of valence particles to an excited $^{56}$Ni core. The same conclusion has been drawn by Otsuka *et al.* [26] in Monte Carlo shell model calculations. In this context, it should be emphasized that small but significant differences in the calculations can only be tested through high precision data. Such a critical evaluation was not possible with the precision of previous data, which in fact showed better agreement with the $t=0$ calculations (Fig. 8).

The calculated $B(E2)$ values exhibit a similar behavior (Fig. 9). The magnitude of the $B(E2)$'s steadily increases with the number of particle-hole excitations but finally converges at $t \simeq 5$ as shown by the full calculation for $^{64}$Ni. The small deviations from the experimental data at the $t=5$ level might be attributed to an underestimation of the effective charge for protons and neutrons used in the calculations, $e_{eff}(\pi) = 1.5e$, $e_{eff}(\nu) = 0.5e$, and/or to a lack of quadrupole strength in the residual interaction. It should be emphasized that the general trend of the data is very well reproduced by the calculations. It is noted that the new lifetime measurement for $^{60}$Ni$(2_1^+)$ brings the experimental $B(E2)$ much closer to the calculated value. Hence the peaking of the $B(E2)$ values is shifted from $^{60}$Ni to neighboring $^{62}$Ni in accordance with the calculation.

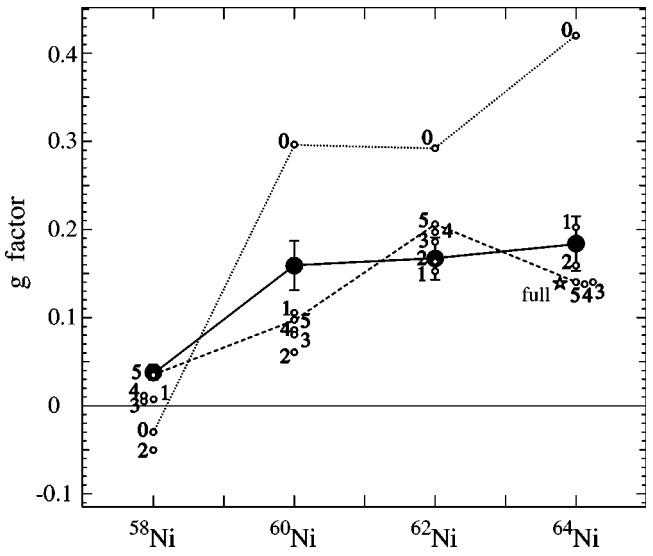


FIG. 8. Experimental $g$ factors of $2_1^+$ states (solid points) are compared with results from shell model calculations in which the number $t$ of nucleons excited from the $0f_{7/2}$ shell into the remaining $fp$ shell orbits (open points) was varied. The result of a full calculation for $^{64}$Ni is marked by a star. Lines are drawn to guide the eye.

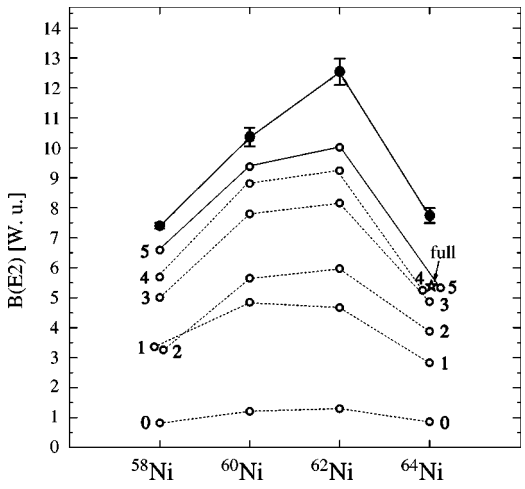


FIG. 9. Experimental $B(E2)$'s of $(2_1^+ \rightarrow 0_1^+)$ in Weisskopf units (solid points) are compared with results from shell model calculations in which the number $t$ of nucleons excited from the $0f_{7/2}$ shell into the remaining $fp$ shell orbits (open points) is increased. The result of a full calculation for $^{64}$Ni is marked by a star. Lines are drawn to guide the eye.

## V. SUMMARY AND CONCLUSIONS

Summarizing the present work, it has been clearly shown that the new technique of projectile Coulomb excitation in inverse kinematics combined with transient magnetic fields provides spectroscopic information of high precision and reliability. This finding is especially characterized by the fact that, in the measurements of series of isotopes like in the present case, the same target can be used while the nuclei of interest are provided by the ion source of accelerators and through perfect mass separation of the accelerated ions. The high precision achieved by this technique allows the detection of subtle effects in nuclear structure and a critical testing of large scale shell model calculations. This strength was particularly exploited in recent measurements of small but significant differences in the core polarization between odd and even $N=28$ isotones [3]. Similarly, in the present case, only with the experimental precision provided by the new technique, was it possible to show that former calculations of the $g$ factor of $^{58}$Ni$(2_1^+)$ did not agree with the data. The rather sophisticated calculations by Mooy and Glaudemans [4] and by Nakada *et al.* [6] yielded $g=-0.05$ and $-0.09$, respectively, clearly negative, and in disagreement with the present result.

Measurements of lifetimes yielded, for the first time, definite values for the $4_1^+$ states of $^{58}$Ni and $^{64}$Ni. Whereas the lifetimes of most states studied were found to be significantly larger than those quoted in the literature, the known $^{62}$Ni$(2_1^+)$ value was precisely confirmed. The magnitude of the $B(E2)$ values deduced for the $(2_1^+ \rightarrow 0_1^+)$ transitions and their dependence on neutron number indicate some collective behavior. It is noteworthy that the collectivity reaches its maximum precisely at the middle of the $fp$ shell (beyond the $^{56}$Ni core) where the number of particles and holes is equal. As a consequence of the gradual filling of the $fp$ shell orbits the amount of collectivity is reduced as shown by the decrease of $B(E2)$ which is further supplemented by recent results for the neutron-rich $^{66}$Ni and $^{68}$Ni [27].

In summary of the theoretical situation, both $g$ factors and $B(E2)$'s of the first $2^+$ states of stable Ni isotopes are well reproduced by shell model calculations in a rather large configuration space. The surrender of an inert $^{56}$Ni core through the excitation of more than two particles from the $0f_{7/2}$ shell is revealing of the complex structure pertaining to even these semiclosed shell nuclei. This scenario is a necessary ingredient in an explanation of the positive $g$ factor of the $^{58}$Ni$(2_1^+)$ state.

## ACKNOWLEDGMENTS

The authors are thankful to the operators of the Tandem accelerator at Munich for their assistance throughout the measurements. Support by the BMBF and the Deutsche Forschungsgemeinschaft is acknowledged.

[1] R. Ernst, K.-H. Speidel, O. Kenn, U. Nachum, J. Gerber, P. Maier-Komor, N. Benczer-Koller, G. Jakob, G. Kumbartzki, L. Zamick, and F. Nowacki, Phys. Rev. Lett. **84**, 416 (2000).
[2] R. Ernst, K.-H. Speidel, O. Kenn, A. Gohla, U. Nachum, J. Gerber, P. Maier-Komor, N. Benczer-Koller, G. Kumbartzki, G. Jakob, L. Zamick, and F. Nowacki, Phys. Rev. C **62**, 024305 (2000).
[3] K.-H. Speidel, R. Ernst, O. Kenn, J. Gerber, P. Maier-Komor, N. Benczer-Koller, G. Kumbartzki, L. Zamick, M.S. Fayache, and Y.Y. Sharon, Phys. Rev. C **62**, 031302(R) (2000).
[4] R.B.M. Mooy and P.W.M. Glaudemans, Z. Phys. A **312**, 59 (1983).
[5] T. Mizusaki, T. Otsuka, Y. Utsuno, N. Honma, and T. Sebe, Phys. Rev. C **59**, R1846 (1999).
[6] H. Nakada, T. Sebe, and T. Otsuka, Nucl. Phys. **A571**, 467 (1994).
[7] M. Hass, N. Benczer-Koller, J.M. Brennan, H.T. King, and P. Goode, Phys. Rev. C **17**, 997 (1978).
[8] P. Raghavan, At. Data Nucl. Data Tables **42**, 189 (1989).
[9] K.-H. Speidel, N. Benczer-Koller, G. Kumbartzki, C. Barton, A. Gelberg, J. Holden, G. Jakob, N. Matt, R.H. Mayer, M. Satteson, R. Tanczyn, and L. Weissman, Phys. Rev. C **57**, 2181 (1998).
[10] G. Jakob, N. Benczer-Koller, J. Holden, G. Kumbartzki, T.J. Mertzimekis, K.-H. Speidel, C.W. Beausang, and R. Krücken, Phys. Lett. B **468**, 13 (1999).
[11] O. Kenn, K.-H. Speidel, R. Ernst, J. Gerber, N. Benczer-Koller, G. Kumbartzki, P. Maier-Komor, and F. Nowacki, Phys. Rev. C **63**, 021302(R) (2001).
[12] P. Maier-Komor, K.-H. Speidel, and A. Stolarz, Nucl. Instrum. Methods Phys. Res. A **334**, 191 (1993).
[13] E. Mathiak, K.A. Eberhard, J.G. Cramer, H.H. Rossner, J. Stettmaier, and A. Weidinger, Nucl. Phys. **A259**, 129 (1976).
[14] O. Kenn, K.-H. Speidel, R. Ernst, S. Wagner, S. Schielke, J.

Gerber, and P. Maier-Komor (unpublished).
[15] F.J. Ziegler, J. Biersack, and U. Littmark, *The Stopping and Range of Ions in Solids* (Pergamon, Oxford, 1985), Vol. 1.
[16] J.C. Wells and N.R. Johnson, program LINESHAPE, 1994, ORNL.
[17] R. Bhat, Nucl. Data Sheets **80**, 789 (1997).
[18] M.M. King, Nucl. Data Sheets **69**, 1 (1993).
[19] M.M. King, Nucl. Data Sheets **60**, 337 (1990).
[20] Balraj Singh, Nucl. Data Sheets **78**, 395 (1996).
[21] G. Jakob, J. Cub, K.-H. Speidel, S. Kremeyer, H. Busch, U. Grabowy, A. Gohla, O. Jessensky, and J. Gerber, Z. Phys. D: At., Mol. Clusters **32**, 7 (1994).
[22] K.-H. Speidel, U. Reuter, J. Cub, W. Karle, F. Passek, H. Busch, S. Kremeyer, and J. Gerber, Z. Phys. D: At., Mol. Clusters **22**, 371 (1991).
[23] R.E. Horstman, J.L. Eberhardt, H.A. Doubt, C.M.E. Otten, and G. Van Middelkoop, Nucl. Phys. **A248**, 291 (1975).
[24] E. Caurier, computer code ANTOINE, Strasbourg, 1989.
[25] A. Poves and A. Zuker, Phys. Rep. **70**, 235 (1981).
[26] T. Otsuka, M. Honma, and T. Mizusaki, Phys. Rev. Lett. **81**, 1588 (1998).
[27] H. Grawe (private communication); (unpublished).